



Dynamics of Localized Unimodal Patterns in Reaction-Diffusion Systems for Cell Polarization by Extracellular Signaling

Kuwamura, Masataka
Seirin-Lee, Sungrim
Ei, Shin-ichiro

(Citation)

SIAM Journal on Applied Mathematics, 78(6):3238-3257

(Issue Date)

2018

(Resource Type)

journal article

(Version)

Version of Record

(Rights)

© 2018, Society for Industrial and Applied Mathematics

(URL)

<https://hdl.handle.net/20.500.14094/90005510>



DYNAMICS OF LOCALIZED UNIMODAL PATTERNS IN REACTION-DIFFUSION SYSTEMS FOR CELL POLARIZATION BY EXTRACELLULAR SIGNALING*

MASATAKA KUWAMURA[†], SUNGRIM SEIRIN-LEE[‡], AND SHIN-ICHIRO EI[§]

Abstract. In this paper, we study the dynamics of a localized unimodal pattern in reaction-diffusion systems with mass conservation, which are mathematical models for the polarity formation of cells. Our result provides a quantitatively precise characterization of the motion of the localized unimodal pattern, which suggests that the location of polarity peaks can be determined universally in a site where the maximal extracellular signal is present regardless of the details of the signaling pathways.

Key words. reaction-diffusion system, localized unimodal pattern, cell polarity, extracellular signaling

AMS subject classifications. 35K57, 92B05

DOI. 10.1137/18M1163749

1. Introduction. Cell polarity is a general phenomenon observed in many stages of development processes where it is used for regulating cell migration, cell aggregation, or cell functions by inducing a different differentiation between two daughter cells. For example, eukaryotic cells such as neutrophils and *Dictyostelium* cells generate a polarity pattern to determine and change their migration direction to where the polarity pattern is established and positioned via a direct response of the extracellular biochemical gradient, referred to as chemotaxis [4, 20, 22]. These cells detect a gradient of the attractant, and polarize and migrate rapidly toward the highest concentration of the chemoattractant.

Similar to polarity formation via chemotaxis, in a cell division process at the early developmental stage, several intracellular substrates within a mother cell are spontaneously distributed asymmetrically in both the membrane and cytosol before cell division, which are then transferred to two daughter cells. This ultimately leads to a diversity of cells with different sizes, shapes, and functions [8, 24, 25]. This process is called asymmetric cell division, in which the polarity formation of proteins in the membrane is considered to play a core role. In asymmetric division, the polarities are formed as two mutually exclusive domains, and the positioning of the polarity domains is a critical factor in determining the specific destiny of the daughter cell. It is widely known that this positioning can be regulated by the direct signal from the contacted neighboring cell, and it has been suggested that the positioning of a specific polarity domain may be induced by a direct signal affecting the translocating rate of

*Received by the editors January 3, 2018; accepted for publication (in revised form) September 28, 2018; published electronically December 4, 2018.

<http://www.siam.org/journals/siap/78-6/M116374.html>

Funding: The first, second, and third authors were supported in part by the JSPS KAKENHI (C) 16K0527, (B) 16K17643, and (B) 26310212, respectively. Moreover, the second and third authors were supported by the JST PRESTO JPMJPR16E2 and CREST JPMJCR14D3, respectively.

[†]Faculty of Human Development, Kobe University, Tsurukabuto 3-11, Nada-ku, Kobe 657-8501, Japan (kuwamura@main.h.kobe-u.ac.jp).

[‡]Department of Mathematics, Hiroshima University, Higashi-hiroshima 739-8530, Japan (seirin@hiroshima-u.ac.jp).

[§]Department of Mathematics, Hokkaido University, Sapporo 060-0810, Japan (Eichiro@math.sci.hokudai.ac.jp).

protein from cytosol to the membrane [1, 24].

To understand the general mechanism of cell polarization, many mathematical models have been proposed, as shown in a survey paper [12] (see also [23] for recent information). Considering the fact that the diffusion-driven (Turing) instability indicates the onset of pattern formation, [11, 20] proposed a conceptual model of a reaction-diffusion system:

$$(1.1) \quad \begin{cases} \dot{u} &= d_1 u_{xx} - \gamma_1 f(u, v), \\ \dot{v} &= d_2 v_{xx} + \gamma_2 f(u, v), \end{cases}$$

where u and v denote the concentrations of two internal chemicals in a cell; u and v correspond to chemicals in the membrane and cytosol, respectively. Since the diffusion in cytosol is faster than that in the membrane, the diffusion coefficients d_1 and d_2 are positive constants satisfying the condition

$$(1.2) \quad d_2 > d_1,$$

and the reaction rates γ_1 and γ_2 are positive constants. We consider (1.1) on an interval $I = (-K/2, K/2)$ for $K > 0$ under the periodic boundary condition, which implies that

$$\int_I (\gamma_2 u(x, t) + \gamma_1 v(x, t)) dx \equiv \int_I (\gamma_2 u(x, 0) + \gamma_1 v(x, 0)) dx$$

holds for any (smooth) solutions of (1.1), i.e., the (weighted) total mass of u and v is conserved in a cell. Therefore, (1.1) is called a reaction-diffusion system with mass conservation.

According to [11, 20], for appropriate functions f , a homogeneous equilibrium can be destabilized through the same mechanism as the diffusion-driven destabilization, and hence solutions with initial values near the destabilized equilibrium exhibit sinusoidal transient patterns. Moreover, by virtue of the aforementioned mass conservation, the solutions eventually approach a localized unimodal pattern (spike). This series of dynamics can be biologically interpreted as the spontaneous establishment of cell polarity inside a cell. Moreover, under appropriate assumptions, it was proved in [13, 18, 19] that any solution converges to an equilibrium, and that every stable equilibrium must be constant or unimodal.

However, as seen in [1, 4, 22], the positioning of cell polarization is regulated by direct extracellular signals transferred from the neighboring cell or the concentration of the chemoattractant. These phenomena have been suggested by different mathematical models in [20, 24], but they can be described by a general system such as

$$(1.3) \quad \begin{cases} \dot{u} &= d_1 u_{xx} - \gamma_1 \{f(u, v) + \varepsilon g(x, u, v)\}, \\ \dot{v} &= d_2 v_{xx} + \gamma_2 \{f(u, v) + \varepsilon g(x, u, v)\} \end{cases}$$

on the interval $I = (-K/2, K/2)$ under the periodic boundary condition. We suppose that the perturbation term g is expressed as

$$(1.4) \quad g(x, u, v) = -g_1(u, v)g_2(x).$$

When g_1 is constant, (1.3) can be written as

$$\begin{cases} \dot{u} &= d_1 u_{xx} - \gamma_1 \{f(u, v) - \varepsilon g(x)\}, \\ \dot{v} &= d_2 v_{xx} + \gamma_2 \{f(u, v) - \varepsilon g(x)\}, \end{cases}$$

which gives a model defined on a domain with spatial inhomogeneity induced by extracellular signals. When a spatial inhomogeneity is incorporated into a parameter of the reaction term f in (1.1), say μ , in such a way that $\mu = \mu_0 + \varepsilon\mu_1(x)$, we obtain (1.3) by applying the Taylor expansion in ε to (1.1). Hence, (1.3) can be considered as a general reaction-diffusion model that describes the cell polarity dynamics induced by extracellular signals. The reaction-diffusion models in [20, 24] are examples of (1.3).

The purpose of this paper is to investigate the dynamics of a localized unimodal pattern in (1.3), which is regarded as an equilibrium of the unperturbed system (1.1). We rigorously derive the equation of motion of the localized pattern, which shows that the localized pattern moves to the maximum point of $g_2(x)$ under natural assumptions. This result gives a quantitatively precise characterization of the motion of the localized unimodal pattern. From the viewpoint of biology, the result proposes conditions under which the location of a polarity peak is determined in the site where the maximal extracellular signal is present.

The remainder of this paper is organized as follows. In section 2, we propose some basic assumptions of our theory on the basis of biological background knowledge and known mathematical results. In section 3, we prepare materials for mathematical analysis. We consider reaction-diffusion systems as an evolution equation on a Hilbert space based on the theory of infinite dimensional dynamical systems. In section 4, we derive the equation of motion for a localized unimodal pattern (spike) in the perturbed reaction-diffusion system (1.3). Moreover, we show that the localized unimodal pattern moves to the maximum point of $g_2(x)$ which represents the spatial inhomogeneity. Section 5 describes the application of our results to two biological models [20, 24, 25] which are based on biologically different contents of polarity positioning such as direct cell-to-cell contacting or long-range signals via chemotaxis. We show that the position of the polarity peak can be precisely determined, which suggests a method for detecting the exact position of a polarity pattern by means of quantitative data of extracellular signals. Moreover, we note that these models exhibit similar dynamics in spite of having biologically different mechanisms. Concluding remarks are presented in section 6.

2. Basic assumptions. In this section, we propose some assumptions on the basis of biological background knowledge and known mathematical results. First, we suppose the existence and stability of a localized unimodal pattern in (1.1).

Assumption 2.1. System (1.1) has a stable equilibrium $S(x) = (p(x), q(x))$ satisfying the following conditions:

- (i) p and q are even periodic functions with period K .
- (ii) p and q are strictly decreasing and increasing, respectively, in x for $0 \leq x \leq K/2$.

The condition that p and q are even functions is natural because (1.1) is invariant under the transformation $x \rightarrow -x$. Moreover, we note that $S(x - c)$ is a stable equilibrium of (1.1) for any $c \in \mathbf{R}$ under the periodic boundary condition. In other words, (1.1) is proposed under the condition that the spatial domain is homogeneous and the parameters are independent of the spatial variable x . Furthermore, we can remove the condition that q is strictly increasing in x for $0 \leq x \leq K/2$, as seen in the proofs of Lemmas 3.1 and 3.2 in the next section.

Next, we propose assumptions concerning the perturbation term g in (1.3), which describes a spatial inhomogeneity.

Assumption 2.2. g_1 and g_2 satisfy the following properties:

- (i) $g_1 \geq 0$ ($g_1 \not\equiv 0$).
- (ii) g_2 is an even periodic function with the period K .
- (iii) g_2 is strictly decreasing in x for $0 \leq x \leq K/2$.

From conditions (ii) and (iii), g_2 has a unique maximum at $x = 0$, which means that a stimulus is given at $x = 0$. Moreover, the condition that g_2 is an even function may be removed. Namely, conditions (ii) and (iii) may be replaced by the conditions (ii') g_2 is a periodic function with the period K , and (iii') g_2 is strictly increasing in x for $-K/2 \leq x \leq 0$ and decreasing for $0 \leq x \leq K/2$. However, we adopt conditions (ii) and (iii) because these conditions enable us to perform mathematical analysis easily, and the reaction-diffusion models in [20, 24] satisfy them. Furthermore, we cannot remove the strictness from condition (iii), as shown in [20, Figure 4E]. Finally, it should be noted that $g_2 \geq 0$ is not required; the sign of $g_1(u, v)$ and $g'_2(x)$ plays a key role in our mathematical analysis.

In this paper, we investigate conditions under which the localized unimodal pattern moves to $x = 0$ translationally in the x -direction in the perturbed system (1.3), i.e., a solution of (1.3) with an initial value in a small neighborhood of $S(x - c)$ for some $c \in \mathbf{R}$ approaches a stable equilibrium approximated by $S(x)$.

3. Preliminaries. In this section, we briefly mention some properties of $S(x)$ that are useful for mathematical analysis. Moreover, we consider the semiflow defined by (1.1) and (1.3), and the linearized operator of the right-hand side of (1.1) at $S(x)$. Finally, we mention an important property of g_2 for mathematical analysis.

LEMMA 3.1.

$$(3.1) \quad d_1\gamma_2p + d_2\gamma_1q \equiv \text{Const.}$$

Proof. Since $S(x) = (p(x), q(x))$ is an equilibrium of (1.1), we have

$$d_1p_{xx} - \gamma_1f(p, q) = 0, \quad d_2q_{xx} + \gamma_2f(p, q) = 0,$$

which leads to $(d_1\gamma_2p + d_2\gamma_1q)_{xx} \equiv 0$. Noting that p and q are even functions, we have $(d_1\gamma_2p + d_2\gamma_1q)_x \equiv 0$ because $p_x(0) = q_x(0) = 0$. Therefore, we see that (3.1) holds. \square

LEMMA 3.2. *There exists an odd periodic function $w(x)$ with the period K such that*

$$(3.2) \quad S_x(x) = w(x) \begin{pmatrix} d_2\gamma_1 \\ -d_1\gamma_2 \end{pmatrix}$$

holds, where $w(x) < 0$ for $0 < x < K/2$.

Proof. From Lemma 3.1, we have $d_1\gamma_2p_x + d_2\gamma_1q_x = 0$. Therefore, when we set $w(x) := p_x/(d_2\gamma_1)$, we see that the assertion of this lemma is true. \square

We rewrite (1.1) and (1.3) as evolution equations on a Hilbert space $L^2(I) \times L^2(I)$, respectively, as follows:

$$(3.3) \quad \mathbf{u}_t = \mathcal{L}(\mathbf{u}), \quad \mathbf{u} = (u, v)$$

and

$$(3.4) \quad \mathbf{u}_t = \mathcal{L}(\mathbf{u}) + \varepsilon G(x, \mathbf{u}), \quad \mathbf{u} = (u, v),$$

where

$$\mathcal{L}(\mathbf{u}) = \begin{pmatrix} d_1 u_{xx} - \gamma_1 f(u, v) \\ d_2 v_{xx} + \gamma_2 f(u, v) \end{pmatrix} \quad \text{and} \quad G(x, \mathbf{u}) = \begin{pmatrix} -\gamma_1 g(x, u, v) \\ \gamma_2 g(x, u, v) \end{pmatrix}.$$

PROPOSITION 3.3. *Equations (3.3) and (3.4) define a semiflow on a hyperplane X_ξ in $L^2(I) \times L^2(I)$, where*

$$X_\xi = \{ \mathbf{u} \in L^2(I) \times L^2(I) \mid \langle \mathbf{u}, \mathbf{a} \rangle = \xi \}$$

for some $\xi \in \mathbf{R}$, and

$$\mathbf{a} = \frac{1}{\sqrt{K(\gamma_1^2 + \gamma_2^2)}} \begin{pmatrix} \gamma_2 \\ \gamma_1 \end{pmatrix}, \quad \langle \mathbf{a}, \mathbf{a} \rangle = 1.$$

Proof. Noting the periodic boundary condition, it follows from (1.1) and (1.3) that

$$\frac{d}{dt} \int_I (\gamma_2 u + \gamma_1 v) dx = \left[d_1 \gamma_2 u_x + d_2 \gamma_1 v_x \right]_{-K/2}^{K/2} = 0$$

holds for solutions of (1.1) and (1.3). This implies that

$$\frac{d}{dt} \langle \mathbf{u}, \mathbf{a} \rangle = 0$$

holds for solutions of (3.3) and (3.4). Therefore, we see that the assertion of this proposition is true. \square

Hereafter, we denote $S(x) \in X_\xi$ by $S(x; \xi)$; that is, $S = S(x; \xi)$ satisfies

$$(3.5) \quad \mathcal{L}(S) = 0$$

and

$$(3.6) \quad \langle S, \mathbf{a} \rangle = \xi.$$

For simplicity, we use S instead of $S(x; \xi)$ unless any confusion occurs. Let us denote by \tilde{L} the linearized operator of the right-hand side of (3.3) at $S \in X_\xi$. It follows from Proposition 3.3 that \tilde{L} is defined on a subspace X in $L^2(I) \times L^2(I)$, where

$$X = \{ \mathbf{u} \in L^2(I) \times L^2(I) \mid \langle \mathbf{u}, \mathbf{a} \rangle = 0 \}.$$

That is, $\tilde{L} = L|_X : X \rightarrow X$ is a restriction of $L : L^2(I) \times L^2(I) \rightarrow L^2(I) \times L^2(I)$, which is defined by

$$(3.7) \quad L = \begin{pmatrix} d_1 & 0 \\ 0 & d_2 \end{pmatrix} \partial_x^2 + \begin{pmatrix} -\gamma_1 \tilde{f}_u & -\gamma_1 \tilde{f}_v \\ \gamma_2 \tilde{f}_u & \gamma_2 \tilde{f}_v \end{pmatrix},$$

where $\tilde{f}_u = f_u(p, q)$, $\tilde{f}_v = f_v(p, q)$, and $S = (p, q) \in X_\xi$. Since $p(x)$ and $q(x)$ are periodic functions with the period K , we have $\langle S_x, \mathbf{a} \rangle = 0$. Moreover, differentiating (3.6) in ξ , we have $\langle S_\xi, \mathbf{a} \rangle = 1$. Therefore, we see that $S_x \in X$ and $S_\xi \notin X$. On the other hand, differentiating (3.5) in x , we have

$$(3.8) \quad LS_x = \tilde{L}S_x = 0.$$

Therefore, $\tilde{L} : X \rightarrow X$ has an eigenvalue 0 and its associated eigenfunction S_x .

Assumption 3.4.

- (i) 0 is a simple eigenvalue of \tilde{L} .
- (ii) $\operatorname{Re}(\sigma(\tilde{L}) \setminus \{0\}) < -\delta$ for some $\delta > 0$.

This assumption is indispensable in rigorously guaranteeing the validity of the equation of motion of a localized unimodal pattern (spike). Here, as seen in [5] and the theory of infinite dimensional dynamical systems [10], we allow this assumption under the situation that a localized unimodal pattern moves translationally in the x -direction, as shown in numerical simulations in section 5.

PROPOSITION 3.5. *Let $\tilde{L}^* : X \rightarrow X$ be the adjoint operator of $\tilde{L} : X \rightarrow X$. Then, \tilde{L}^* has a simple eigenvalue 0 and its associated eigenfunction is given by*

$$\Phi^* = \begin{pmatrix} \frac{-w(x) + \gamma_2 \varphi_2^*(x)}{\gamma_1} \\ \varphi_2^*(x) \end{pmatrix} \in X,$$

where

$$\varphi_2^*(x) = h_1(x) + Ax$$

is an odd function, and

$$(3.9) \quad h_1(x) = \int_0^x \int_0^y h_2(s) ds dy, \quad A = \int_0^{K/2} \left(\frac{2y}{K} - 1 \right) h_2(y) dy,$$

and

$$(3.10) \quad h_2(x) = -\frac{1}{d_2} \tilde{f}_v w(x), \quad \tilde{f}_v = f_v(p, q), \quad S = (p, q) \in X_\xi.$$

Proof. First, we note that Φ^* satisfying $L^* \Phi^* = 0$ automatically satisfies $\tilde{L}^* \Phi^* = 0$ due to the relation $\tilde{L}^* \mathbf{u} := L^* \mathbf{u} - \langle L^* \mathbf{u}, \mathbf{a} \rangle \mathbf{a}$. By (3.7), the adjoint operator of $L : L^2(I) \times L^2(I) \rightarrow L^2(I) \times L^2(I)$ is given by

$$L^* = \begin{pmatrix} d_1 & 0 \\ 0 & d_2 \end{pmatrix} \partial_x^2 + \begin{pmatrix} -\gamma_1 \tilde{f}_u & \gamma_2 \tilde{f}_u \\ -\gamma_1 \tilde{f}_v & \gamma_2 \tilde{f}_v \end{pmatrix},$$

where $\tilde{f}_u = f_u(p, q)$, $\tilde{f}_v = f_v(p, q)$, and $S = (p, q) \in X_\xi$. Let $\Phi^* = (\varphi_1^*, \varphi_2^*)^T$. Then, we have

$$d_1 \frac{d^2 \varphi_1^*}{dx^2} + \tilde{f}_u (-\gamma_1 \varphi_1^* + \gamma_2 \varphi_2^*) = 0 \quad \text{and} \quad d_2 \frac{d^2 \varphi_2^*}{dx^2} + \tilde{f}_v (-\gamma_1 \varphi_1^* + \gamma_2 \varphi_2^*) = 0.$$

Putting

$$(3.11) \quad \psi^* := -\gamma_1 \varphi_1^* + \gamma_2 \varphi_2^*,$$

we see that ψ^* and φ_2^* satisfy

$$(3.12) \quad d_1 \frac{d^2 \psi^*}{dx^2} - d_1 \gamma_2 \frac{d^2 \varphi_2^*}{dx^2} - \gamma_1 \tilde{f}_u \psi^* = 0 \quad \text{and} \quad d_2 \frac{d^2 \varphi_2^*}{dx^2} + \tilde{f}_v \psi^* = 0.$$

Since

$$(3.13) \quad \frac{d^2 \varphi_2^*}{dx^2} = -\frac{\tilde{f}_v}{d_2} \psi^*$$

from the second equation of (3.12), substituting (3.13) into the first equation of (3.12), we obtain

$$d_1 \frac{d^2 \psi^*}{dx^2} - \left\{ \gamma_1 \tilde{f}_u - \frac{d_1 \gamma_2}{d_2} \tilde{f}_v \right\} \psi^* = 0.$$

On the other hand, it follows from (3.2), (3.7), and (3.8) that

$$LS_x = \begin{pmatrix} d_1 d_2 \gamma_1 w_{xx} - \{d_2 \gamma_1^2 \tilde{f}_u - d_1 \gamma_1 \gamma_2 \tilde{f}_v\} w \\ -d_1 d_2 \gamma_2 w_{xx} + \{d_2 \gamma_1 \gamma_2 \tilde{f}_u - d_1 \gamma_2^2 \tilde{f}_v\} w \end{pmatrix} = \begin{pmatrix} 0 \\ 0 \end{pmatrix},$$

which leads to

$$d_1 \frac{d^2 w}{dx^2} - \left\{ \gamma_1 \tilde{f}_u - \frac{d_1 \gamma_2}{d_2} \tilde{f}_v \right\} w = 0.$$

Hence, we find

$$(3.14) \quad \psi^* = w,$$

and it follows from (3.13) that

$$\frac{d^2 \varphi_2^*}{dx^2} = h_2,$$

where $h_2 = h_2(x)$ is given by (3.10). Therefore, we have

$$\varphi_2^*(x) = \int_0^x \int_0^y h_2(s) ds dy + Ax + B.$$

We choose $B = 0$ in such a way that φ_2^* is an odd function. Moreover, noting $\varphi_2^*(-K/2) = \varphi_2^*(K/2)$ because φ_2^* is a periodic function with the period K , we have

$$\begin{aligned} A &= \frac{1}{K} \left\{ \int_0^{-K/2} \int_0^y h_2(s) ds dy - \int_0^{K/2} \int_0^y h_2(s) ds dy \right\} \\ &= -\frac{1}{K} \int_{-K/2}^{K/2} \int_0^y h_2(s) ds dy. \end{aligned}$$

Since h_2 is an odd function by Assumption 2.1(i) and Lemma 3.2, we have

$$\begin{aligned} A &= -\frac{2}{K} \int_0^{K/2} \int_0^y h_2(s) ds dy \\ &= -\frac{2}{K} \left\{ \left[y \int_0^y h_2(s) ds \right]_0^{K/2} - \int_0^{K/2} y h_2(y) dy \right\} \\ &= \int_0^{K/2} \left(\frac{2y}{K} - 1 \right) h_2(y) dy. \end{aligned}$$

Therefore, we obtain $\varphi_2^*(x) = h_1(x) + Ax$, where $h_1(x)$ and A are given by (3.9). Moreover, by (3.11) and (3.14), we have $\varphi_1^*(x) = (-w(x) + \gamma_2 \varphi_2^*(x))/\gamma_1$. Furthermore, φ_1^* and φ_2^* are odd functions because w is an odd function by Lemma 3.2. Hence, we have

$$\langle \Phi^*, \mathbf{a} \rangle = \frac{1}{\sqrt{K(\gamma_1^2 + \gamma_2^2)}} \int_{-K/2}^{K/2} (\gamma_2 \varphi_1^*(x) + \gamma_1 \varphi_2^*(x)) dx = 0,$$

which implies that $\Phi^* \in X$. □

PROPOSITION 3.6. $\varphi_2^*(x) > 0$ for $0 < x < K/2$ if (i) $h_2(x) < 0$ for $0 < x < K/2$ or (ii) there exists $\alpha \in (0, K/2)$ such that $h_2(x) < 0$ for $0 < x < \alpha$ and $h_2(x) > 0$ for $\alpha < x < K/2$, and

$$\int_0^{K/2} x h_2(x) dx < 0.$$

Proof. We note that

$$\frac{d^2 \varphi_2^*}{dx^2} = h_2 \quad (0 < x < K/2)$$

by Proposition 3.5, and that $\varphi_2^*(0) = \varphi_2^*(K/2) = 0$ because φ_2^* is an odd periodic function with the period K . Therefore, φ_2^* is upwards convex on $(0, K/2)$ if $h_2(x) < 0$, which implies that $\varphi_2^*(x) > 0$ for $0 < x < K/2$ under condition (i). Moreover, it follows from Proposition 3.5 that

$$\frac{d\varphi_2^*}{dx}(K/2) = \int_0^{K/2} h_2(x) dx + A = \frac{2}{K} \int_0^{K/2} x h_2(x) dx,$$

which implies that $\varphi_2^*(x) > 0$ for $0 < x < K/2$ under condition (ii). \square

Finally, we mention an important property of $g_2(x)$ in the perturbation term g , which is used in the next section.

LEMMA 3.7. $g_2(x - \ell) > g_2(x + \ell)$ for $0 < x < K/2$ and $0 < \ell < K/2$.

Proof. Noting that $-K/2 < x - \ell < K/2$ and $0 < x + \ell < K$ for $0 < x < K/2$ and $0 < \ell < K/2$, we consider the following four cases: (i) $0 < x - \ell < K/2$, $0 < x + \ell < K/2$, (ii) $0 < x - \ell < K/2$, $K/2 \leq x + \ell < K$, (iii) $-K/2 < x - \ell \leq 0$, $0 < x + \ell < K/2$, and (iv) $-K/2 < x - \ell \leq 0$, $K/2 \leq x + \ell < K$. Here, we treat only case (iv) because the other cases are easier and can be treated in a similar manner.

Since g_2 is an even periodic function with the period K , we have $g_2(x - \ell) = g_2(\ell - x)$ and $g_2(x + \ell) = g_2(x + \ell - K) = g_2(K - x - \ell)$. Noting that g_2 is decreasing on $[0, K/2]$, we see that

$$g_2(x - \ell) - g_2(x + \ell) = g_2(\ell - x) - g_2(K - x - \ell) > 0$$

holds for case (iv) because $0 \leq \ell - x < K/2$, $0 < K - x - \ell \leq K/2$, and $(K - x - \ell) - (\ell - x) = K - 2\ell > 0$. \square

4. Dynamics of localized unimodal pattern. In this section, we investigate the dynamics of (1.3) around a manifold $M = \{S(x - \ell) \mid \ell \in \mathbf{R}\} \subset X_\xi$. According to the theory of infinite dimensional dynamical systems [10] and numerical simulations performed in [20], we expect that solutions of (1.3) with an initial value in a sufficiently small neighborhood of M move along M and converge to a stable equilibrium approximated by $S(x)$.

Let $\mathbf{u} = \mathbf{u}(x, t)$ be a solution of (3.4), which is an evolution equation on X_ξ defined by (1.3). Noting that M is parameterized by ℓ , let

$$(4.1) \quad \mathbf{u}(x, t) = S(x - \ell(t)) + V(x - \ell(t), t) = S(z) + V(z, t),$$

where $z = x - \ell(t)$ and $V \in X$. Since solutions of (1.3) around M can be expressed by (4.1), we consider that the equation of $\ell(t)$ determines the dynamics of (1.3) around M under Assumption 3.4.

Differentiating (4.1) with respect to t , we have

$$\mathbf{u}_t = -\dot{\ell}S_z + V_t - \dot{\ell}V_z, \quad \dot{\ell} = d\ell/dt.$$

On the other hand, substituting (4.1) into the right-hand side of (3.4), we have

$$\begin{aligned} \mathcal{L}(\mathbf{u}) + \varepsilon G(x, \mathbf{u}) &= \mathcal{L}(S + V) + \varepsilon G(z + \ell, S + V) \\ &= \mathcal{L}(S) + \tilde{L}V + O(\|V\|^2) + \varepsilon G(z + \ell, S) + O(\varepsilon\|V\|) \\ &= \tilde{L}V + \varepsilon G(z + \ell, S) + O(\varepsilon^2 + \|V\|^2). \end{aligned}$$

Therefore, we have

$$V_t - \dot{\ell}V_z = \tilde{L}V + \dot{\ell}S_z + \varepsilon G(z + \ell, S) + O(\varepsilon^2 + \|V\|^2).$$

By neglecting higher-order error terms, we obtain

$$(4.2) \quad V_t = \tilde{L}V + \dot{\ell}S_z + \varepsilon G(z + \ell, S)$$

if $\max(\|V\|, \|V_z\|) = O(\varepsilon)$ and $|\dot{\ell}| = O(\varepsilon)$. According to [10], the condition that solutions of (4.2) are uniformly bounded in X under Assumption 3.4 is

$$\langle \dot{\ell}S_z + \varepsilon G(z + \ell, S), \Phi^* \rangle = 0.$$

Hence, we obtain

$$(4.3) \quad \frac{d\ell}{dt} = \varepsilon H(\ell) + O(\varepsilon^2),$$

where

$$H(\ell) = -\frac{J(\ell)}{\langle S_z, \Phi^* \rangle} \quad \text{and} \quad J(\ell) = \langle G(z + \ell, S), \Phi^* \rangle.$$

This equation determines the dynamics of (1.3) around M . Noting that $|\dot{\ell}| = O(\varepsilon)$ by (4.3), we have $\max(\|V\|, \|V_z\|) = O(\varepsilon)$ by (4.2) and $V \in H^1(I) \times H^1(I)$ under Assumption 3.4. This implies that the validity of (4.2) and (4.3) can be rigorously guaranteed by applying the same lines of argument in [5] based on the theory of infinite dimensional dynamical systems.

Remark 4.1. In many practical applications, the constant independent of ε included in the error term denoted by $O(\varepsilon^2)$ in (4.3) can be estimated by $O(Ke^{-K})$. This is due to the fact that $p(x)$ and $q(x)$ converge exponentially as $|x|$ goes to infinity. Consequently, for sufficiently small values of ε , the error term of (4.3) can be negligible if K is sufficiently large.

PROPOSITION 4.2. *If $\varphi_2^*(x) > 0$ for $0 < x < K/2$, then*

$$\langle S_z, \Phi^* \rangle = -2d_2 \int_0^{K/2} w^2(z)dz + 2(d_2 - d_1)\gamma_2 \int_0^{K/2} w(z)\varphi_2^*(z)dz < 0.$$

Proof. It follows from Lemma 3.2 and Proposition 3.5 that

$$\begin{aligned} \langle S_z, \Phi^* \rangle &= \left\langle w \begin{pmatrix} d_2\gamma_1 \\ -d_1\gamma_2 \end{pmatrix}, \begin{pmatrix} \gamma_1^{-1}(-w + \gamma_2\varphi_2^*) \\ \varphi_2^* \end{pmatrix} \right\rangle \\ &= \int_{-K/2}^{K/2} (d_2w(z)(-w(z) + \gamma_2\varphi_2^*(z)) - d_1\gamma_2w(z)\varphi_2^*(z))dz \\ &= -d_2 \int_{-K/2}^{K/2} w^2(z)dz + (d_2 - d_1)\gamma_2 \int_{-K/2}^{K/2} w(z)\varphi_2^*(z)dz. \end{aligned}$$

Noting that w and φ_2^* are odd functions, we have

$$\langle S_z, \Phi^* \rangle = -2d_2 \int_0^{K/2} w^2(z) dz + 2(d_2 - d_1)\gamma_2 \int_0^{K/2} w(z)\varphi_2^*(z) dz < 0$$

because $w(z) < 0$ and $\varphi_2^*(z) > 0$ for $0 < z < K/2$ and (1.2). \square

PROPOSITION 4.3. $J(\ell)$ is an odd periodic function with the period K , and

$$J(\ell) = \int_0^{K/2} \rho(z) \{g_2(z + \ell) - g_2(z - \ell)\} dz,$$

where $\rho(z) = -g_1(p(z), q(z))w(z)$. Moreover, $J(0) = J(-K/2) = J(K/2) = 0$ and $J(\ell) < 0$ for $0 < \ell < K/2$.

Proof. It follows from (1.4) and Proposition 3.5 that

$$\begin{aligned} J(\ell) &= \langle G(z + \ell, S), \Phi^* \rangle = \left\langle \begin{pmatrix} -\gamma_1 g \\ \gamma_2 g \end{pmatrix}, \begin{pmatrix} \gamma_1^{-1}(-w + \gamma_2 \varphi_2^*) \\ \varphi_2^* \end{pmatrix} \right\rangle \\ &= \int_{-K/2}^{K/2} g(z + \ell, p(z), q(z)) w(z) dz \\ &= - \int_{-K/2}^{K/2} g_1(p(z), q(z)) g_2(z + \ell) w(z) dz = \int_{-K/2}^{K/2} \rho(z) g_2(z + \ell) dz. \end{aligned}$$

It follows from Assumptions 2.1 and 2.2 and Lemma 3.2 that ρ is an odd periodic function with the period K , and that $\rho(z) > 0$ for $0 < z < K/2$. Therefore, we have

$$\begin{aligned} J(\ell) &= \int_{-K/2}^{K/2} \rho(z) g_2(z + \ell) dz \\ &= \int_{-K/2}^0 \rho(z) g_2(z + \ell) dz + \int_0^{K/2} \rho(z) g_2(z + \ell) dz \\ &= \int_0^{K/2} \rho(z) \{g_2(z + \ell) - g_2(z - \ell)\} dz < 0 \end{aligned}$$

for $0 < \ell < K/2$ by Lemma 3.7. Moreover, noting that ρ is an odd periodic function with the period K , we see that $J(\ell)$ is an odd periodic function with the period K , because g_2 is an even periodic function with the period K according to Assumption 2.2. This implies that $J(0) = J(-K/2) = J(K/2) = 0$. \square

From Lemma 3.2 and Propositions 3.5, 3.6, 4.2, and 4.3, we obtain the following result which characterizes the dynamics of localized unimodal pattern.

THEOREM 4.4. $d\ell/dt = \varepsilon H(\ell)$ has only two equilibria $\ell = 0$ and $\ell = K/2 (= -K/2)$. Moreover, $\ell = 0$ is stable and $\ell = K/2$ is unstable if $\varphi_2^*(x) > 0$ for $0 < x < K/2$. In particular, $\ell = 0$ is stable and $\ell = K/2$ is unstable under any of the following conditions: (i) $f_v(p(x), q(x)) < 0$ for $0 < x < K/2$, (ii) there exists $\alpha \in (0, K/2)$ such that $f_v(p(x), q(x)) < 0$ for $0 < x < \alpha$ and $f_v(p(x), q(x)) > 0$ for $\alpha < x < K/2$, and

$$\int_0^{K/2} x f_v(p(x), q(x)) p'(x) dx > 0 \quad \text{or} \quad \int_0^{K/2} x f_v(p(x), q(x)) q'(x) dx < 0.$$

Although condition (i) is practical, it is rather strict. In contrast, condition (ii) is an improved version of condition (i) so as to extend the scope of application of Theorem 4.4.

Remark 4.5. If we replace $g_1 \geq 0$ by $g_1 \leq 0$ in condition (i) of Assumption 2.2, the assertion of Theorem 4.4 is changed so that $\ell = 0$ is unstable and $\ell = K/2$ is stable. This suggests that $g_1 \geq 0$ and $g_1 \leq 0$ correspond, respectively, to the positive and negative feedback effects of extracellular signals in cell polarization [24].

5. Examples. In this section, we show some examples of reaction-diffusion models used in [11, 20, 24, 25] for understanding cell polarization.

Example 5.1.

$$(5.1) \quad \begin{cases} \dot{u} &= d_1 u_{xx} - \gamma \{F(u) - v - \varepsilon \chi(x)\}, \\ \dot{v} &= d_2 v_{xx} + \gamma \{F(u) - v - \varepsilon \chi(x)\}, \end{cases}$$

where

$$(5.2) \quad F(u) = \left(a_0 + \frac{a_4}{a_1 + a_2 u + a_3 u^2} \right) u$$

and

$$(5.3) \quad \chi(x) = b_0 \cos \left(\frac{2\pi x}{K} \right) + b_1$$

with nonnegative constants b_k ($k = 1, 2$) and a_j ($j = 0, 1, 2, 3, 4$) satisfying $a_1^2 + a_2^2 + a_3^2 \neq 0$.

This is a simplification (dimensionless form) of a model that has been developed in [24] for studying extracellular signal effects on the dynamics of PAR (partitioning-defective proteins) polarity patterns arising in asymmetric cell division. The perturbation term $\chi(x)$ denotes the effect of an extracellular signal from a neighboring cell; b_0 represents the maximal strength of a signal centered at $x = 0$. Note that (5.1) can be obtained from (1.3) by setting $f(u, v) = F(u) - v$ and $g(x, u, v) = -g_1(u, v)g_2(x)$ with $g_1(u, v) \equiv 1$ and $g_2(x) = \chi(x)$, where $F(u)$ is given by (5.2). Moreover, it is easy to see that Assumption 2.2 is satisfied in this case.

We numerically solve (5.1) on $I = (-K/2, K/2)$ under the periodic boundary condition to investigate the dynamics of a localized unimodal pattern. Our simulations are based on a standard pseudospectral method [6, 9], and the numerical scheme is presented in [16, Appendix]. According to [24, Table A1], we choose the following dimensionless values of parameters:

$$(5.4) \quad a_0 = 0.3, a_1 = 0.25, a_2 = 0.1, a_3 = 1.0, a_4 = 6.225, \gamma = 0.2.$$

First, we numerically solve (5.1) for $\varepsilon = 0$, i.e.,

$$(5.5) \quad \begin{cases} \dot{u} &= d_1 u_{xx} - \gamma \{F(u) - v\}, \\ \dot{v} &= d_2 v_{xx} + \gamma \{F(u) - v\} \end{cases}$$

with an initial value $(u_0(x), v_0(x)) = (u_0 + \varepsilon_1(x), v_0 + \varepsilon_2(x))$, where (u_0, v_0) is a spatially homogeneous equilibrium of (5.5), and $(\varepsilon_1(x), \varepsilon_2(x))$ is a sufficiently small disturbance. This model has been introduced as a spontaneous polarization model

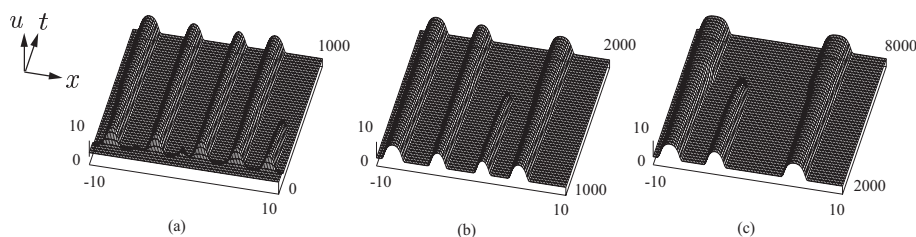


FIG. 1. Spatial patterns with multiple peaks of (5.5) when $K = 20.0$. The values of $u(x, t)$ on $-10.0 \leq x \leq 10.0$ and (a) $0 \leq t \leq 1000$, (b) $1000 \leq t \leq 2000$, (c) $2000 \leq t \leq 8000$ are represented by 3D graphs. The spatial profiles of $v(x, t)$ are omitted here because the spatial variation of $v(x, t)$ for each t is relatively small compared to that of $u(x, t)$, and the local minimal points of $v(x, t)$, corresponding to the peaks of $u(x, t)$, are rather difficult to see. The values of the parameters are given by (5.4) and those of diffusion coefficients are given by $d_1 = 0.0048$ and $d_2 = 0.288$. Moreover, the initial value is given by $(2.0 + \varepsilon_1(x), 3.4 + \varepsilon_2(x))$, where $\varepsilon_1(x)$ and $\varepsilon_2(x)$ are independent uniform pseudorandom numbers in $[-0.005, 0.005]$ for each $x \in [-10.0, 10.0]$.

in [24, 25], and its mathematical aspects have been studied in [13, 18, 19]. According to dimensionless values given in [24, Table A1], we choose $(u_0, v_0) \approx (2.0, 3.4)$ and the values of diffusion coefficients as $d_1 = 0.0048$ and $d_2 = 0.288$.

Figure 1 shows that spatial patterns with multiple peaks appear when the interval length is given by $K = 20.0$, which is equivalent to that of [24, Table A1] under the spatial rescaling $x \rightarrow 20x$. As reported in [11, 20], a spatially homogeneous equilibrium can be destabilized through the same mechanism as the diffusion-driven (Turing) instability, and spatial patterns with multiple peaks appear. Moreover, the number of peaks decreases, and the solutions eventually approach a simple localized unimodal pattern.

Although it was proved in [13, 18, 19] that spatial patterns with multiple peaks are unstable, numerical solutions are often trapped in a neighborhood of these patterns because of round-off errors in numerical computations. In our simulations, almost every numerical solution cannot leave a spatial pattern with two peaks when $K = 20.0$. Therefore, this value of K is not desirable to confirm the validity of our mathematical results in section 3. On the other hand, the number of peaks of such spatial patterns maintained for a sufficiently long time depends on system size K . In fact, an early stage of dynamics generating these spatial patterns is due to the diffusion-driven (Turing) instability, and the number of peaks decreases as K decreases. In our simulations, a localized unimodal pattern (spatial pattern with a single peak) eventually appears for $1.2 \lesssim K \lesssim 13.6$. Here, noting Remark 4.1, we choose $K = 10.0$ to obtain $(p(x), q(x))$ satisfying Assumption 2.1 as shown in Figure 2.

Next, we numerically solve (5.1) for $\varepsilon = 0.01$. The initial value is given by a localized unimodal pattern obtained by a translation of the one shown in Figure 2. Here, the position of the peak of the initial localized pattern is given by $\ell = \ell_0 = -2.5$. The values of parameters in (5.3) are given by $b_0 = b_1 = 1.0$. Figure 3 shows that the numerical solution starting from $S(x - \ell_0) = (p(x - \ell_0), q(x - \ell_0))$ translationally moves to $x = 0$ in the x -direction. Notice that the velocity of this translational movement is not constant. The numerical result presented in Figure 3 is supported by Theorem 4.4. In fact, condition (i) in Theorem 4.4 holds by

$$\frac{\partial}{\partial v} f(u, v) = \frac{\partial}{\partial v} (F(u) - v) \equiv -1 < 0,$$

and hence $\ell = 0$ is a stable equilibrium of (4.3).

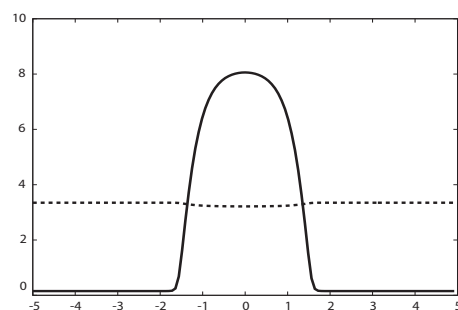


FIG. 2. The spatial profiles of $p(x)$ and $q(x)$ for $K = 10.0$. The solid and dashed lines represent $p(x)$ and $q(x)$, respectively.

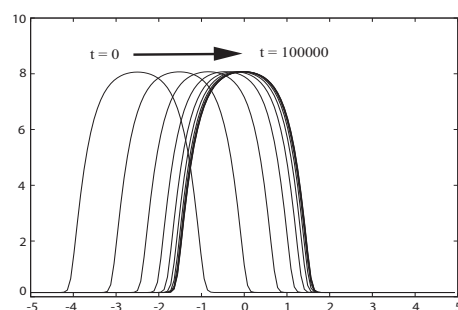


FIG. 3. The motion of a localized unimodal pattern of (5.1) for $\varepsilon = 0.01$. The spatial profiles of $u(x, t)$ are given by the graphs of $u(x, t)$ on $-5 \leq x \leq 5$ for $t = 10000n$ ($n \in \mathbf{Z}$, $0 \leq n \leq 10$). The spatial profiles of $v(x, t)$ are omitted here because the spatial variation of $v(x, t)$ for each t is relatively small compared to that of $u(x, t)$, and the motion of the minimal point of $v(x, t)$ is rather difficult to see. Notice that the velocity of this translational movement is not constant. The values of the parameters are given by (5.4) and $b_0 = b_1 = 1.0$, and those of diffusion coefficients are given by $d_1 = 0.0048$ and $d_2 = 0.288$.

In what follows, we give a concrete expression of (4.3). By Lemma 3.2 and Propositions 3.5, 4.2, and 4.3, we have

$$J(\ell) = -\frac{1}{d_2\gamma} \int_0^{K/2} p'(z) \{\chi(z+\ell) - \chi(z-\ell)\} dz,$$

$$\langle S_z, \Phi^* \rangle = -\frac{2}{d_2\gamma^2} \int_0^{K/2} p'(z)^2 dz + \frac{2(d_2 - d_1)}{d_2} \int_0^{K/2} p'(z) \varphi_2^*(z) dz,$$

and

$$\varphi_2^*(x) = \frac{1}{d_2^2\gamma} \left(\int_0^x p(z) dz - \frac{2x}{K} \int_0^{K/2} p(z) dz \right).$$

Noting $d_1 p_{xx} - \gamma \{F(p) - q\} = 0$ and $p'(0) = p'(K/2) = 0$ since p is an even periodic

function with period K , by using integration by parts, we have

$$\begin{aligned} J(\ell) &= -\frac{1}{d_2\gamma} \left(p(K/2) \{ \chi(K/2 + \ell) - \chi(K/2 - \ell) \} \right. \\ &\quad \left. - \int_0^{K/2} p(z) \{ \chi'(z + \ell) - \chi'(z - \ell) \} dz \right) \\ &= -\frac{4\pi b_0}{d_2\gamma K} \sin\left(\frac{2\pi\ell}{K}\right) \int_0^{K/2} p(z) \cos\left(\frac{2\pi z}{K}\right) dz \end{aligned}$$

and

$$\begin{aligned} \langle S_z, \Phi^* \rangle &= \frac{2}{d_1 d_2 \gamma} \int_0^{K/2} \{ F(p(z)) - q(z) \} p(z) dz \\ &\quad + \frac{2(d_2 - d_1)}{d_2^3 \gamma} \left\{ \frac{2}{K} \left(\int_0^{K/2} p(z) dz \right)^2 - \int_0^{K/2} p^2(z) dz \right\}. \end{aligned}$$

Therefore, we see that (4.3) is given by

$$(5.6) \quad \frac{d\ell}{dt} = -\varepsilon C \sin\left(\frac{2\pi\ell}{K}\right) + O(\varepsilon^2),$$

where C is a positive constant independent of b_1 . Notice that $Ke^{-K} \approx 4.5 \times 10^{-4}$ (see Remark 4.1) and $C \approx 1.0 \times 10^{-2}$ by using the numerical data of $p(x)$ and $q(x)$ in Figure 2. We numerically solve (5.6) with initial value $\ell(0) = -2.5$ by using a standard scheme based on the Runge–Kutta method. Figure 4 shows that the motion of a localized unimodal pattern presented in Figure 3 is determined by (5.6) with $\ell(0) = -2.5$.

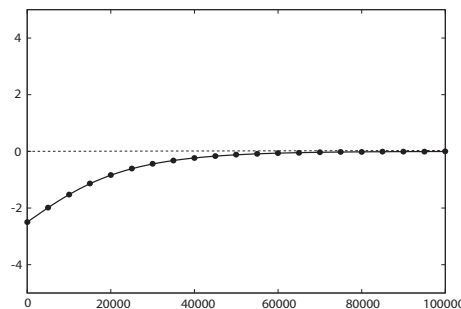


FIG. 4. A comparison of theory and numerical simulations. The solid and dashed lines represent a solution of (5.6) with initial value $\ell(0) = -2.5$ and its limit as $t \rightarrow \infty$ given by $\ell = 0$, respectively. The dots represent the maximal point of $u(x, t)$ for $t = 5000n$ ($n \in \mathbf{Z}$, $0 \leq n \leq 20$).

Thus, Example 5.1 demonstrates that the dynamics of a localized unimodal pattern of (1.3) is determined by the ODE (4.3), which implies that a localized unimodal pattern of (1.3) moves to the maximum point of $g_2(x)$.

Remark 5.2. We apply our mathematical results presented in previous sections, which are based on Assumptions 2.1 and 3.4. In general, it would not be easy to

rigorously check these assumptions. For this example, we can verify that these assumptions hold for sufficiently small d_1/d_2 when $a_0 = a_2 = 0$ and $\gamma = 1$. In fact, it was shown in [18, Corollary 1.2] that any stable equilibrium of (5.5) is spatially homogeneous or it has a single peak. Therefore, noting the fact that solutions of the Neumann problem on $(0, K/2)$ can be regarded as those of the periodic boundary problem on $(-K/2, K/2)$ by the reflection with respect to the vertical axis, by using [3, Theorem 1.1, Corollary 1.2, and Remark 1.6], we see that Assumption 2.1 holds for sufficiently small d_1/d_2 . Moreover, it follows from [18, Corollary 1.1] that $\sigma(\tilde{L})$ is a discrete set on \mathbf{R} . Since $S(x)$ is stable, noting the periodic boundary condition, we see that Assumption 3.4(ii) holds, and that \tilde{L} has an eigenvalue 0 which is generically simple [14]. Hence, Assumption 3.4(i) generically holds.

Example 5.3.

$$(5.7) \quad \begin{cases} \dot{u} &= d_1 u_{xx} - \gamma(F(u+v) - v), \\ \dot{v} &= d_2 v_{xx} + \gamma(F(u+v) - v), \end{cases}$$

where $F(s) = s/(1+as)^2$ and

$$a = a_0 \left\{ 1 + \varepsilon \cos \left(\frac{2\pi(x-c)}{K} \right) \right\}$$

with $a_0 > 0$, $\gamma > 0$, and $-K/2 \leq c < K/2$.

This conceptual model is used in [20] for understanding extracellular signal effects on the dynamics of Rho GTPases polarity patterns. Applying the Taylor expansion in ε to (5.7), we have

$$(5.8) \quad \begin{cases} \dot{u} &= d_1 u_{xx} - \gamma\{f(u, v) + \varepsilon g(x, u, v)\}, \\ \dot{v} &= d_2 v_{xx} + \gamma\{f(u, v) + \varepsilon g(x, u, v)\}, \end{cases}$$

where

$$f(u, v) = F_0(u+v) - v, \quad F_0(s) = s/(1+a_0s)^2$$

and $g(x, u, v) = -g_1(u+v)g_2(x)$,

$$g_1(s) = \frac{2s^2}{(1+a_0s)^3}, \quad g_2(x) = a_0 \cos \left(\frac{2\pi(x-c)}{K} \right).$$

Notice that (5.8) gives a good approximation for (5.7).

First, we consider (5.7) on $I = (-K/2, K/2)$ under the periodic boundary condition. According to [20], we numerically solve (5.7) with an initial value $(u_0(x), v_0(x)) \equiv (1.0, 1.0)$ for $\varepsilon = 0.01$ under the parameter values

$$(5.9) \quad a_0 = 0.7, \quad \gamma = 2.5, \quad d_1 = 0.01, \quad d_2 = 1.0$$

and the interval length $K = 10.0$. When $c = -2.0$, the numerical solution converges to $(p_0(x), q_0(x))$, which is a localized unimodal pattern with the maximum at $x = -2.0$. Setting $c = 0$, we numerically solve (5.7) with an initial value $(p_0(x), q_0(x))$ under the same parameter values and interval length as (5.9) and $K = 10.0$. Figure 5 shows that the maximal point of the numerical solution moves from $x = -2.0$ to $x = 0$. The procedure and result of this numerical simulation are the same as in [20, Figure 3H].

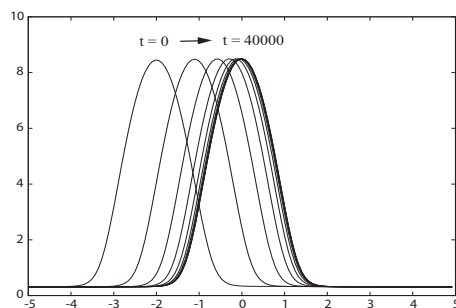


FIG. 5. The motion of a localized unimodal pattern of (5.7) for $\varepsilon = 0.01$. The spatial profiles of $u(x, t)$ are given by the graphs of $u(x, t)$ on $-5 \leq x \leq 5$ for $t = 4000n$ ($n \in \mathbf{Z}$, $0 \leq n \leq 10$). The spatial profiles of $v(x, t)$ are omitted here because the spatial variation of $v(x, t)$ for each t is relatively small compared to that of $u(x, t)$, and the motion of the minimal point of $v(x, t)$ is rather difficult to see. Notice that the velocity of this translational movement is not constant. The values of the parameters and diffusion coefficients are given by (5.9).

Remark 5.4. The trigger of the formation of $(p_0(x), q_0(x))$ is not due to the diffusion-driven destabilization (Turing instability). In fact, $(u_0, v_0) = (1.0, 1.0)$ is not an equilibrium of an ODE system obtained by dropping diffusion terms from (5.7).

Next, we consider (5.8) on $I = (-K/2, K/2)$ under the periodic boundary condition when $c = 0$. Here, we suppose that (5.8) for $\varepsilon = 0$ has a localized unimodal pattern (spike) $S(x) = (p(x), q(x))$ satisfying Assumption 2.1 and

$$(5.10) \quad \lim_{K \rightarrow \infty} (p(K/2) + q(K/2)) = \alpha \quad \text{for some } \alpha > 0.$$

Then, $p(x) + q(x) > 0$ holds for $0 < x < K/2$. In fact, it follows from Lemma 3.2 that

$$\begin{aligned} \frac{d}{dx}(p(x) + q(x)) &= p'(x) + q'(x) \\ &= (d_2 w(x)) + (-d_1 w(x)) = (d_2 - d_1)w(x) < 0 \end{aligned}$$

holds for $0 < x < K/2$. Therefore, $p(x) + q(x)$ is decreasing in x for $0 < x < K/2$. Hence, it follows from (5.10) that $p(x) + q(x) > 0$ holds for $0 < x < K/2$. Since

$$\frac{\partial}{\partial v} f(u, v) = \frac{\partial}{\partial v} (F_0(u + v) - v) = F'_0(u + v) - 1,$$

we can easily check that $f_v(p(x), q(x)) < 0$ holds for $0 < x < K/2$, which implies that condition (i) of Theorem 4.4 holds under the condition (5.10).

In the same way as in Example 5.1, when $c = 0$, we can numerically investigate the dynamics of a localized unimodal pattern in (5.8) under the parameter values (5.9) and interval length $K = 10.0$.

Figure 6 shows the localized unimodal pattern $S(x)$ of (5.8) for $\varepsilon = 0$ when $c = 0$. This numerical result supports the fact that $p(x)$ and $q(x)$ satisfy condition (5.10). Therefore, we consider that condition (i) of Theorem 4.4 holds. Figure 7 shows that the maximal point of the numerical solution moves from $x = -2.0$ to $x = 0$. This numerical result is supported by Theorem 4.4.

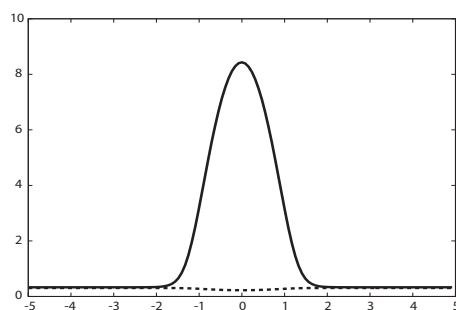


FIG. 6. The spatial profiles of $p(x)$ and $q(x)$ of (5.8) for $\varepsilon = 0$. The solid and dashed lines represent $p(x)$ and $q(x)$, respectively.

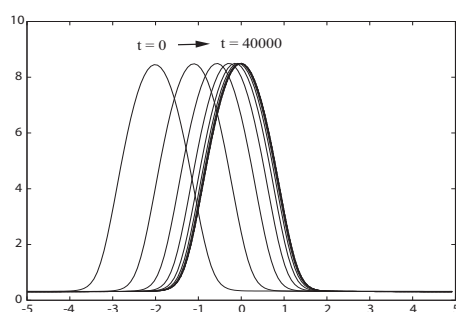


FIG. 7. The motion of a localized unimodal pattern of (5.8) for $\varepsilon = 0.01$. The spatial profiles of $u(x, t)$ are given by the graphs of $u(x, t)$ on $-5 \leq x \leq 5$ for $t = 4000n$ ($n \in \mathbf{Z}$, $0 \leq n \leq 10$). The spatial profiles of $v(x, t)$ are omitted here because the spatial variation of $v(x, t)$ for each t is relatively small compared to that of $u(x, t)$, and the motion of the minimal point of $v(x, t)$ is rather difficult to see. The values of the parameters and diffusion coefficients are given by (5.9).

Since

$$\begin{aligned} J(\ell) &= \int_0^{K/2} \rho(z) \{g_2(z + \ell) - g_2(z - \ell)\} dz \\ &= -2a_0 \sin\left(\frac{2\pi\ell}{K}\right) \int_0^{K/2} \rho(z) \sin\left(\frac{2\pi z}{K}\right) dz, \end{aligned}$$

we find that (4.3) is given by

$$(5.11) \quad \frac{d\ell}{dt} = -\varepsilon C \sin\left(\frac{2\pi\ell}{K}\right) + O(\varepsilon^2),$$

where C is a positive constant. In contrast to Example 5.1, it is rather difficult to precisely obtain the value of C by using the numerical data of $p(x)$ and $q(x)$ in Figure 6. Therefore, we estimate this value by the position of the maximal point of the numerical solution of (5.8), as shown in Figure 7. Consequently, we find $C \approx 0.028$.

Figure 8 shows that the motion of a localized unimodal pattern of (5.7) presented in Figure 5 is determined by (5.11) with $\ell(0) = -2.0$. This result provides a quantitatively precise characterization of the qualitatively reasonable results in [20], which cannot be obtained by a formal argument based on biological insights.

Here, we mention biological implications of Examples 5.1 and 5.3. As seen in (5.6) and (5.11), the ODE (4.3) which determines the polarity position can be expressed

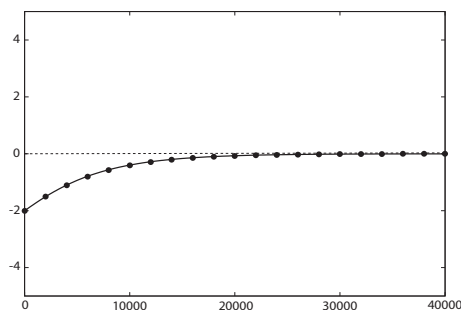


FIG. 8. A comparison of theory and numerical simulations. The solid and dashed lines represent a solution of (5.11) with initial value $\ell(0) = -2.0$ and its limit as $t \rightarrow \infty$ given by $\ell = 0$, respectively. The dots represent the maximal point of $u(x, t)$ of (5.7) for $t = 2000n$ ($n \in \mathbf{Z}$, $0 \leq n \leq 20$).

in terms of the sine function if $g_2(x)$ is expressed in terms of the cosine function, where $g_2(x)$ represents the spatial inhomogeneity of extracellular signals. It should be noted that the form of (4.3) expressed in terms of the sine function does not depend on $f(u, v)$ which characterizes the intracellular dynamics for spontaneous cell polarization. Moreover, the moving speed of the polarity position attains its maximum at the point where the absolute value of the gradient of $g_2(x)$ attains its maximum because of $(\cos x)' = -\sin x$. However, at present, we do not know whether or not these properties are valid for a general case such that $g_2(x)$ is not expressed in terms of the cosine function.

Asymmetric cell division in the early stage of an embryo (Example 5.1) is a process tightly regulated by the dynamics of the polarity pattern inside a cell [8]. Moreover, this intracellular dynamics is affected by extracellular signals. Therefore, understanding the underlying mechanism of the dynamics of the polarity pattern under the presence of extracellular signals is an indispensable factor in knowing how a cell can control its division position and timing [21]. Considering that the dynamics of the polarity pattern is actually determined by that of the position of the polarity peak, (5.6) and (5.11) in these examples suggest that we could precisely predict the dynamics of the polarity pattern if we could know the details of quantitative data of extracellular signals [23].

Remark 5.5. The models (5.1) and (5.7) are examples satisfying condition (i) of Theorem 4.4. In contrast, the model used in [20],

$$\begin{cases} \dot{u} &= d_1 u_{xx} - \{f(u, v) + \varepsilon g(x, u, v)\}, \\ \dot{v} &= d_2 v_{xx} + \{f(u, v) + \varepsilon g(x, u, v)\}, \end{cases}$$

is an example satisfying condition (ii) of Theorem 4.4, where $f(u, v) = -a_1(u + v)\{(\alpha u + v)(u + v) - a_2\}$ and $g(x, u, v) = -a_1(u + v)a_E(x)$ with positive constants a_1, a_2, α and a bounded continuous function $a_E(x)$. As seen in [20], this model enables us to perform concrete calculations using elementary functions. However, rather lengthy calculations are required to check condition (ii) of Theorem 4.4. In addition, as seen in [17], we can investigate the dynamics of such reaction-diffusion systems with cubic nonlinear reaction terms through asymptotic and bifurcation analysis. Therefore, we will treat this model in a separate paper [15].

6. Concluding remarks. In this paper, we have studied the dynamics of a localized unimodal pattern in reaction-diffusion systems with mass conservation, which

are mathematical models for the polarity formation of cells. These systems have a spatially nonhomogeneous term in each of their components, which can be regarded as a small perturbation. Our results show that the localized unimodal pattern moves to the maximum point of the spatially nonhomogeneous term under certain conditions, which suggests that the location of the polarity peak can be determined universally in the site where the maximal extracellular signal is present regardless of the details of the signaling pathways.

The cell migration induced by the extracellular gradient signal, namely, chemotaxis, is a general mechanism that arises in the processes of angiogenesis, cancer metastasis, wound healing, inflammation, and embryogenesis [2, 4, 20, 22]. For determining the correct direction of migration, a cell forms a polarity pattern corresponding to the gradient of extracellular signals. Therefore, for understanding the mechanism of cell migration, it is indispensable to determine the location of the polarity peak. Our mathematical result shows that the location of the polarity peak can be determined in the site where the value of the extracellular signal is maximum, suggesting that the cell could detect the exact direction of migration.

Although biological details are different, a similar polarity formation is also shown in asymmetric cell division. In *Caenorhabditis elegans*, a single fertilized egg cell (P0), its daughter cell (P1), and the germline precursors (P2 and P3 cells) are asymmetrically divided, forming two exclusive domains of different partitioning defective proteins, namely PAR-2 and PAR-6, on the membrane. In particular, PAR-2 is a key protein that characterizes the dynamics of the polarity pattern during asymmetric division, so the positioning of the PAR-2 polarity domain is critical in determining the fate of a daughter cell. These features have been studied through biological experiments and mathematical models [7, 11, 20, 24, 25], but a general mechanism for determining the position of the polarity pattern of PAR-2 has not been clarified yet.

The model in Example 5.1 has been formulated to explain how the positive feedback of the extracellular signal transmitter plays a critical role in determining the polarity peak in the extracellular signal site. For this model, we rigorously proved that the position of the polarity peak is determined at the location where the extracellular signal has a maximal signal. Furthermore, Theorem 4.4 suggests that the dynamics of cytosol protein by the influence of the extracellular signal plays a more critical role than that of the membrane protein in determining the position of the polarity peak in the extracellular signal site. Taken together, our analysis provides a viewpoint for understanding a general mechanism by which the positioning of cell polarity can be determined robustly.

Acknowledgments. The authors thank Wataru Kohno and Yuri Bitoh, who were undergraduate and graduate students of the third author, respectively, for their help with numerical experiments related to this paper. Moreover, the authors would like to express their appreciation to the referees for their useful suggestions and comments, which have improved the original manuscript.

REFERENCES

- [1] Y. ARATA, J.-Y. LEE, B. GOLDSTEIN, AND H. SAWA, *Extracellular control of PAR protein localization during asymmetric cell division in the C. elegans embryo*, Development, 137 (2010), pp. 3337–3345.
- [2] Y.-C. CHEN, S. G. ALLEN, P. N. INGRAM, R. BUCKANOVICH, S. D. MERAJVER, AND E. YOON, *Single-cell migration chip for chemotaxis-based microfluidic selection of heterogeneous cell populations*, Sci. Rep., 5 (2015), 9980.

- [3] J. L. CHERN, Y. MORITA, AND T. T. SHIEH, *Asymptotic behavior of equilibrium states of reaction-diffusion systems with mass conservation*, J. Differential Equations, 264 (2018), pp. 550–574.
- [4] C. Y. CHUNG, S. FUNAMOTO, AND R. A. FIRTEL, *Signaling pathways controlling cell polarity and chemotaxis*, Trends Biochem. Sci., 26 (2001), pp. 557–566.
- [5] S.-I. EI, *The motion of weakly interacting pulses in reaction-diffusion systems*, J. Dynam. Differential Equations, 14 (2002), pp. 85–137.
- [6] B. FORNBERG, *A Practical Guide to Pseudospectral Methods*, Cambridge University Press, Cambridge, UK, 1996.
- [7] N. M. GOEHRING, P. K. TRONG, J. S. BOIS, C. CHOWDHURY, E. M. NICOLA, A. A. HYMAN, AND S. W. GRILL, *Polarization of PAR proteins by advective triggering of a pattern-forming system*, Science, 334 (2011), pp. 1137–1141.
- [8] P. GÖNCZY AND L. S. ROSE, *Asymmetric cell division and axis formation in the embryo*, WormBook.org, 2005, <https://doi.org/10.1895/wormbook.1.30.1>.
- [9] D. GOTTLIEB AND S. A. ORSZAG, *Numerical Analysis of Spectral Methods: Theory and Applications*, CBMS-NSF Regional Conf. Ser. in Appl. Math. 26, SIAM, Philadelphia, 1977.
- [10] D. HENRY, *Geometric Theory of Semilinear Parabolic Equations*, Lecture Notes in Math. 840, Springer-Verlag, Berlin, New York, 1981.
- [11] S. ISHIHARA, M. OTSUJI, AND A. MOCHIZUKI, *Transient and steady state of mass-conserved reaction-diffusion systems*, Phys. Rev. E, 75 (2007), 015203.
- [12] A. JILKINE AND L. EDELSTEIN-KESHET, *A comparison of mathematical models for polarization of single eukaryotic cells in response to guided cues*, PLoS Comput. Biol., 3 (2011), e1001121.
- [13] S. JIMBO AND Y. MORITA, *Lyapunov function and spectrum comparison for a reaction-diffusion system with mass conservation*, J. Differential Equations, 255 (2013), pp. 1657–1683.
- [14] T. KATO, *Perturbation Theory for Linear Operators*, 2nd ed., Classics Math., Springer-Verlag, Berlin, 1995.
- [15] M. KUWAMURA AND S.-I. EI, in preparation.
- [16] M. KUWAMURA AND Y. MORITA, *Perturbations and dynamics of reaction-diffusion systems with mass conservation*, Phys. Rev. E, 92 (2015), 012908.
- [17] Y. MORI, A. JILKINE, AND L. EDELSTEIN-KESHET, *Asymptotic and bifurcation analysis of wave-pinning in a reaction-diffusion model for cell polarization*, SIAM J. Appl. Math., 71 (2011), pp. 1401–1427, <https://doi.org/10.1137/10079118X>.
- [18] Y. MORITA, *Spectrum comparison for a conserved reaction-diffusion system with a variational property*, J. Appl. Anal. Comput., 2 (2012), pp. 57–71.
- [19] Y. MORITA AND T. OGAWA, *Stability and bifurcation of nonconstant solutions to a reaction-diffusion system with conservation of mass*, Nonlinearity, 23 (2010), pp. 1387–1411.
- [20] M. OTSUJI, S. ISHIHARA, C. CO, K. KAIBUCHI, A. MOCHIZUKI, AND S. KURODA, *A mass conserved reaction-diffusion system captures properties of cell polarity*, PLoS Comput. Biol., 3 (2007), e108.
- [21] C. PANBIANCO AND M. GOTTA, *Coordinating cell polarity with cell division in space and time*, Trends Cell Biol., 21 (2011), pp. 672–680.
- [22] C. A. PARENT AND T. N. DEVREOTES, *A cell's sense of direction*, Science, 284 (1999), pp. 765–770.
- [23] W. J. RAPPEL AND L. EDELSTEIN-KESHET, *Mechanisms of cell polarization*, Curr. Opin. Syst. Biol., 3 (2017), pp. 43–53.
- [24] S. SEIRIN-LEE, *Positioning of polarity formation by extracellular signaling during asymmetric cell division*, J. Theoret. Biol., 400 (2016), pp. 52–64.
- [25] S. SEIRIN-LEE AND T. SHIBATA, *Self-organization and advective transport in the cell polarity formation for asymmetric cell division*, J. Theoret. Biol., 382 (2015), pp. 1–14.